crystals

MDPI

Article

3D Hierarchical Composites of Hydrotalcite-Coated Carbon Microspheres as Catalysts in Baeyer–Villiger Oxidation Reactions

Marta Estrada-Ruiz, Daniel Cosano *, Dolores Esquivel, Francisco J. Romero-Salguero and José Rafael Ruiz *

Departamento de Química Orgánica, Instituto Químico para la Energía y el Medioambiente (IQUEMA), Facultad de Ciencias, Universidad de Córdoba, Campus de Rabanales, Edificio Marie Curie, 14071 Córdoba, Spain; q92esrum@uco.es (M.E.-R.); q12esmem@uco.es (D.E.); qo2rosaf@uco.es (F.J.R.-S.)
* Correspondence: q92cohid@uco.es (D.C.); qo1ruarj@uco.es (J.R.R.)

Abstract: The use of heterogeneous catalysts is fundamental in the search for sustainable chemical processes. Research on hierarchical materials is a growing field aimed at optimizing the synthesis of catalysts. In this work, layered materials with metals of different cationic ratios and three-dimensional hierarchical structures have been synthesized in a simple and easy way using carbon spheres as support. All materials were characterized with various techniques such as XRF, elemental analysis XRD, FT-IR, SEM, and TEM to study their composition and structure. Finally, these materials were used in the Baeyer–Villiger reaction, which was carried out under optimized conditions. The results showed that the metal ratio was an important factor in the coating process, affecting the catalytic capacity of the materials.

Keywords: carbon microspheres; hydrotalcite; metal ratio; Baeyer–Villiger oxidation

check for updates

Citation: Estrada-Ruiz, M.; Cosano, D.; Esquivel, D.; Romero-Salguero, F.J.; Ruiz, J.R. 3D Hierarchical Composites of Hydrotalcite-Coated Carbon Microspheres as Catalysts in Baeyer–Villiger Oxidation Reactions. *Crystals* **2024**, *14*, 878. https://doi.org/10.3390/cryst14100878

Academic Editors: Ioannis Spanopoulos and Ferdinando Costantino

Received: 5 July 2024
Revised: 27 September 2024
Accepted: 2 October 2024
Published: 5 October 2024

Copyright: © 2024 by the authors. Licensee MDPI, Basel, Switzerland. This article is an open access article distributed under the terms and conditions of the Creative Commons Attribution (CC BY) license (https://creativecommons.org/licenses/by/4.0/).

1. Introduction

One of the key objectives of Green Chemistry is to incorporate the use of eco-friendly reagents and heterogeneous catalysts successfully. This approach aims to reduce environmental harm, enhance process efficiency, and support sustainable chemical practices [1]. A notable example of this synergy is found in the adaptation of the Baeyer–Villiger reaction, where a ketone is oxidized to an ester using an organic peroxide. Originally developed by Baeyer and Villiger, this reaction involved the formation of lactones from menthone and carvomenthone by reacting with a mixture of potassium monopersulfate and sulfuric acid without a solvent, operating in a homogeneous phase [2]. Later, this reaction was applied for the oxidation of aldehydes with other oxidants such as peracids or peroxides. However, the use of peracids is limited due to their hazardous effect on nature, making treatment with H_2O_2 an attractive alternative that has been enhanced in recent research [3]. Although hydrogen peroxide is less active than peracids, its use requires a catalyst to improve the reaction yield. That fact has led to an increase in the number of studies related to the heterogenization of the Baeyer–Villiger reaction using catalysts. Moreover, the use of catalysts provides simpler operational processes, allows for more economical reagents, and reduces environmental impacts. Several catalysts have been explored for this purpose [4,5], including layered double hydroxides (LDHs), which are also referred to as hydrotalcite-like compounds or simply "hydrotalcites" (HTs) [6–10]. This has resulted in a rise in the number of research efforts directed at enhancing these materials.

Hydrotalcites are particularly versatile due to their unique structural composition, consisting of layers resembling brucite composed of $Mg(OH)_2$ octahedra, and where magnesium cations are centrally located in octahedra coordinated to hydroxyl groups ($OH-$) at their vertices, with these octahedra sharing edges to create stacked layers. In HTs, the layers carry a positive charge as a result of the substitution of some divalent cations (M^{2+})

with trivalent cations (M^{3+}). This way, electroneutrality is achieved due to the presence of anions, which support the structure of the layers by compensating for the positive charge, along with water molecules in the interlayer region. The general chemical formulae for hydrotalcite is $[M(II)_{1-x}\ M(III)_x\ (OH)_2]^{x+}\ [X_{n/x}]^{n-}\cdot mH_2O$, where $M^{(II)}$ and $M^{(III)}$ represent divalent and trivalent metals, respectively, and X denotes the interlayer anion [11–13]. The anion located in the interlayer region can be of organic or inorganic origin. [14]. This structural versatility endows hydrotalcite with a wide range of physicochemical properties, making it suitable for diverse applications in scientific and industrial fields [15,16].

Hydrotalcite being used as catalysts for the Baeyer–Villiger reaction requires the use of a nitrile to react with hydrogen peroxide on their surface, forming peroxycarboximidic acid, the actual oxidizing agent [17,18]. For this reason, the catalytic activity is predominantly limited to the outer surface of the hydrotalcite. Thus, enhancing HT activity involves modifying their surface physicochemical properties. Consequently, numerous researchers have focused their studies on optimizing the synthesis process [15,19].

Recent advances in synthetic techniques have enabled the development of hierarchical three-dimensional hydrotalcites for various applications [20–22]. This new generation of materials includes carbon microsphere-based hydrotalcite composites [23]. Carbon microspheres possess ordered structures that allow for the controlled arrangement of carbon atoms, facilitating specific morphologies such as spherical shapes, tubes, or fibers [24–26]. Carbon surfaces exhibit a porous network with functional groups like hydroxyl (C-OH) and carbonyl (C=O) [27]. These functional groups promote interactions among carbon microspheres, enabling them to be potential nucleation sites for hydrotalcite growth. Hierarchical hydrotalcite structures with carbonaceous materials are typically synthesized using layer-by-layer deposition or in situ growth methods [23], involving coprecipitation from a suspension of carbon. In earlier studies, our team documented the synthesis and structural analysis of silica microspheres covered by Mg/Al hydrotalcite layers [28]. These hybrid materials were subsequently used in the Baeyer–Villiger oxidation of different cyclic ketones using hydrogen peroxide as the oxidant [29].

In this study, we have research about the impact of the ratio of divalent and trivalent metals in the synthesis process of hierarchical materials on carbon microsphere structures, and we evaluated their effectiveness in the Baeyer–Villiger reaction. Our findings highlight the crucial role of metal composition in enhancing catalytic performance and structural integrity, highlighting the importance of inducing homogeneous and compact growth to optimize these properties.

2. Materials and Methods

2.1. Synthesis of Carbon Microspheres (CM)

Carbon microspheres were synthesized using the hydrothermal method. For this process, 22 mmol of D-glucose was added to 25 mL of deionized water; this solution was placed into a stainless Teflon-sealed autoclave with a capacity of 40 mL. The reaction oven was maintained at 160 °C for 24 h. The resulting suspension was then filtered, rinsed with 100 mL of water, and dried overnight at 80 °C in an oven.

2.2. Synthesis of CM@HT Composites

The synthesis of carbon microspheres coated by 3D hierarchical hydrotalcite composites was performed using the previously described in situ coprecipitation method. In a standard synthetic procedure, a solution containing 0.02 mol of $Mg(NO_3)_2\cdot 6H_2O$ and 0.01 mol of $Al(NO_3)_3\cdot 9H_2O$ in 150 mL of deionized water (Mg/Al = 2) was slowly added over 2 h to a solution of 500 mg of carbon microspheres in 500 mL of deionized water. Prior to the addition, the microsphere suspension was sonicated (ultrasound bath: Ultrasons, JP Selecta, 150 W) for 60 min to ensure a uniform dispersion. The pH was adjusted to 9 throughout the process by periodically adding 1 M NaOH while stirring vigorously at 60 °C. After 2 h, the resulting suspension was left to settle at 80 °C for 24 h, then filtered and rinsed with 2 L of deionized water to obtain a solid known as HT. A similar procedure was

used to prepare two other HTs in theorical metal ratios of 3 (0.03 mol of $Mg(NO_3)_2 \cdot 6H_2O$ and 0.01 mol of $Al(NO_3)_3 \cdot 9H_2O$) and 4 (0.04 mol of $Mg(NO_3)_2 \cdot 6H_2O$ and 0.01 mol of $Al(NO_3)_3 \cdot 9H_2O$). The resulting materials were denoted as CM@HT-X, where X represents the specific metal ratio employed.

2.3. Characterization

To determine the metal ratio of the materials, X-ray fluorescence (XRF) spectroscopy was performed using a Rigaku ZSK Primus IV instrument. The amount of carbon was determined through elemental analysis, which was conducted using an EA3000 EuroVector Elemental Analyzer, involving the complete combustion of 10 mg of sample material. To clarify that the structure of the materials was hydrotalcite-like and to assess their crystallinity, X-ray diffraction (XRD) was performed. The patterns were collected over the 2θ range of 5−70° using Cu Kα radiation on a Bruker D8 Discover A25 diffractometer. The lattice parameters were calculated using Bragg's law ($2d_{hkl} \sin \theta = n \lambda$). Peaks at (003), (006), and (110) were utilized to determine the lattice parameters c and a. Parameter c, representing three times the interlayer distance, was computed as $3 \cdot [d_{(003)} + 2d_{(006)}]/2$. In contrast, parameter a, which corresponds to the distance between two adjacent cations in a brucite-like layer of hydrotalcite, was derived from 2·d(110). Crystallite size was determined using the Scherrer equation, $D_{hkl} = R (\lambda / \beta \cos\theta)$. In this equation, R represents the Scherrer constant (0.89), λ denotes the wavelength of the incident X-ray (0.154 nm), β is the peak width at half maximum (in radians), and θ is the Bragg angle. To identify the nature of the interlayer anion and verify the hydrotalcite-like structure of the materials, Fourier transform infrared (FTIR) analyses were performed. FTIR spectra spanning the wavenumber range of 400−4000 cm^{-1} were recorded using a Nicolet Magna IR 500 instrument, with the samples prepared in a KBr matrix as a reference. Finally, to determine the proper hierarchy of the materials, images were analyzed using scanning electron microscopy (SEM) and high-resolution transmission electron microscopy (TEM). SEM images were acquired using a JEOL JSM 7800F microscope operated at 5 kV and a working distance of 10 mm. TEM images were obtained using a JEOL JEM 1400 microscope.

2.4. Bayer–Villiger Reaction

Baeyer–Villiger oxidation was carried out at 90 °C in a temperature-controlled round bottom flask with stirring at 700 rpm. The reaction mixture included 0.012 mol of cyclohexanone, 0.098 mol of benzonitrile, 0.1 mol of 30% hydrogen peroxide solution, and 0.12 g of catalyst. The setup was equipped with a reflux condenser, and samples were taken periodically. The reaction mixtures were analyzed using a Bruker gas chromatograph (450GC) fitted with an Rxi-5Sil MS capillary column (30 m × 0.25 mm ID) and a flame ionization detector (FID).

3. Results and Discussion

3.1. Characterization

3.1.1. Carbon Microsphere (CM)

Figure 1a,b show transmission and scanning electron micrographs of the synthesized carbon microspheres. As observed, the microspheres exhibited a uniform spherical morphology with a diameter of approximately 0.5 μm in all cases. Although they were linked together forming agglomerates, they retained their spherical shape and exhibited smooth, uniform surfaces. The XRD pattern shown in Figure 1c indicates that the microspheres were amorphous. They displayed a wide main peak at 2θ = 21°, which corresponds to the (002) diffraction plane, and a weak peak at 2θ = 40.7°, assigned to the (100) diffraction plane, which is consistent with their amorphous carbonaceous composition [30]. Finally, the chemical structure of the carbon microspheres (CM) was investigated using FT-IR (Figure 1d). The broad band at 3500 cm^{-1}, along with the region between 1000 and 1300 cm^{-1}, corresponds to the O-H stretching vibration (hydroxyl groups). The band at 2920 cm^{-1} was attributed to the C-H stretching of the aliphatic carbon. The bands at 1707 and 1620 cm^{-1}

are assigned to C=O and C=C vibrations, respectively, corroborating the aromatization of glucose during the synthesis process. Lastly, the bands between 850 and 750 cm^{-1}, attributed to out-of-plane C-H aromatic bending vibrations, further indicate that aromatization occurred [31]. In summary, these results confirm that the spheres were correctly synthesized through a hydrothermal treatment.

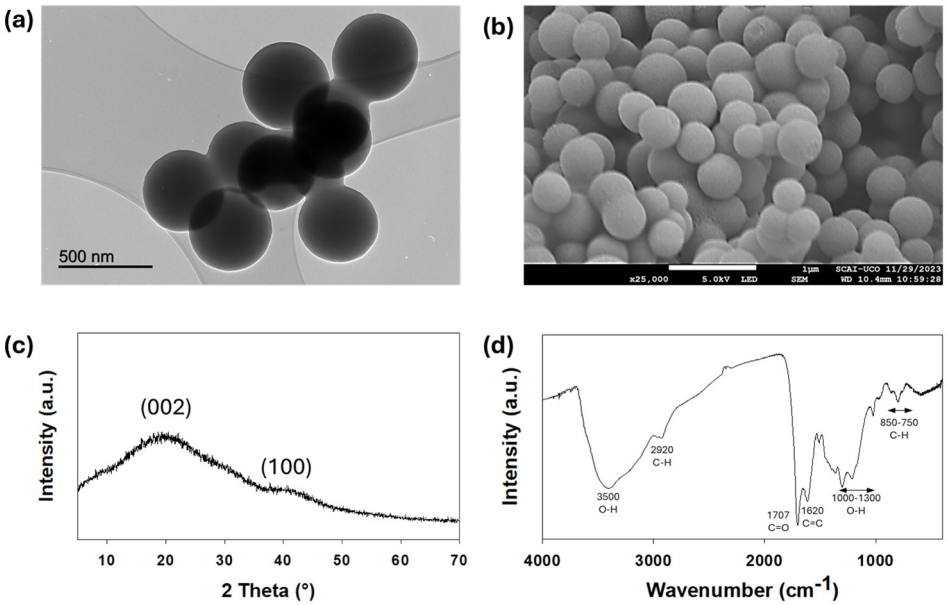

Figure 1. TEM (**a**); SEM (**b**); XRD pattern; (**c**) and IR spectrum (**d**) for the carbon microspheres.

3.1.2. Catalysts (CM@HT-X)

Table 1 shows the chemical composition of each CM@HT-X (X is the Mg/Al ratio) was determined through XRF spectra (Figure S1) and elemental analysis. The experimental values closely matched the theoretical ones, suggesting that the cations were accurately incorporated into the solid phase. As observed, the Mg/Al ratio increased consistently with the addition of more Mg in the synthesis. However, in the case where the Mg proportion is higher, we observed a decrease compared to the theoretical ratio, which could be attributed to the selective dissolution of the magnesium component during the washing of the precipitate with distilled water [32]. Finally, the carbon content in the synthesized materials was determined, and in all cases, the values were around 17%, indicating that the quantity of carbon microspheres remained consistent throughout the synthesis process.

Table 1. Metal ratio, lattice parameters and crystallite for the CM@HT-X.

Catalyst	χ_{ther} [a]	χ_{exp} [b]	%C [c]	d_{003} (Å) [d]	c (Å) [d]	a (Å) [d]	t (nm) [e]
CM@HT-2	0.33	0.34	18	7.8	23.4	3.05	14
CM@HT-3	0.25	0.25	16	7.8	23.4	3.06	14
CM@HT-4	0.20	0.22	17	7.9	23.7	3.07	15

[a]: theoretical metal ratio [χ = Al/(Mg + Al)]; [b]: experimental metal ratio as determined by XRF. [c]: experimental anion as determined by elemental analysis. [d]: Lattice parameters; c and a were calculated from $d_{(003)}$ and $d_{(110)}$ planes, respectively; [e] Crystallite size.

Figure 2 shows the XRD patterns for the synthesized hydrotalcites, all of which exhibited the typical signals of layered materials. We observe narrow and symmetrical peaks at low 2θ values, corresponding to the basal planes (003), (006), and (009), which are parallel to the layers in the hydrotalcite structure. The reflections from these planes indicate regularity in the layer spacing. Meanwhile, the less intense peaks at higher values represent the non-basal planes (012), (015), and (018), which are not parallel to the layers of the

structure. These planes intersect the layers and reflect the three-dimensional arrangement of atoms within the structure. The reflections from these planes tend to be broader and more symmetrical, indicating their dependence on the disorder within the layers or the variability in the distance between atoms in different directions [33]. However, we can observe that the peaks shown in Figure 2 are less symmetrical than those typically represented in these materials. This can be explained by the fact that the layered materials are coating the carbonaceous surface of the microspheres. This effect has already been demonstrated in other articles, where it has been confirmed that the size of the layers is affected by the coating of the materials. In cases where the growth of the hydrotalcites is unrestrained, a considerable increase in layer size is observed [28,33], resulting in the formation of more intense and narrow peaks than those shown in Figure 2. The synthesis using the coprecipitation method results in smaller particle sizes compared to other methods and also allows a more effective coating of carbon microspheres. Additionally, it was observed that this coating effect produces smaller sheet sizes compared to similar syntheses without coating [16]. If we observe the intensity of the diffraction patterns (015) and (018), they are more intense in the CM@HT-2 sample. This difference in intensity could indicate variations in the formation and alignment of the crystals in this sample compared to CM@HT-3 and CM@HT-4. One possible explanation for this higher intensity is the existence of regions in CM@HT-2 with better crystalline ordering in certain planes, resulting in stronger reflections. These more intense peaks suggest that the structure of CM@HT-2 may have fewer restrictions on the arrangement of its layers, allowing for greater variability in crystalline formation. This lower restriction could also indicate that part of the hydrotalcite may be interacting differently with the carbon spheres or forming independently, thus contributing to the more intense reflections observed.

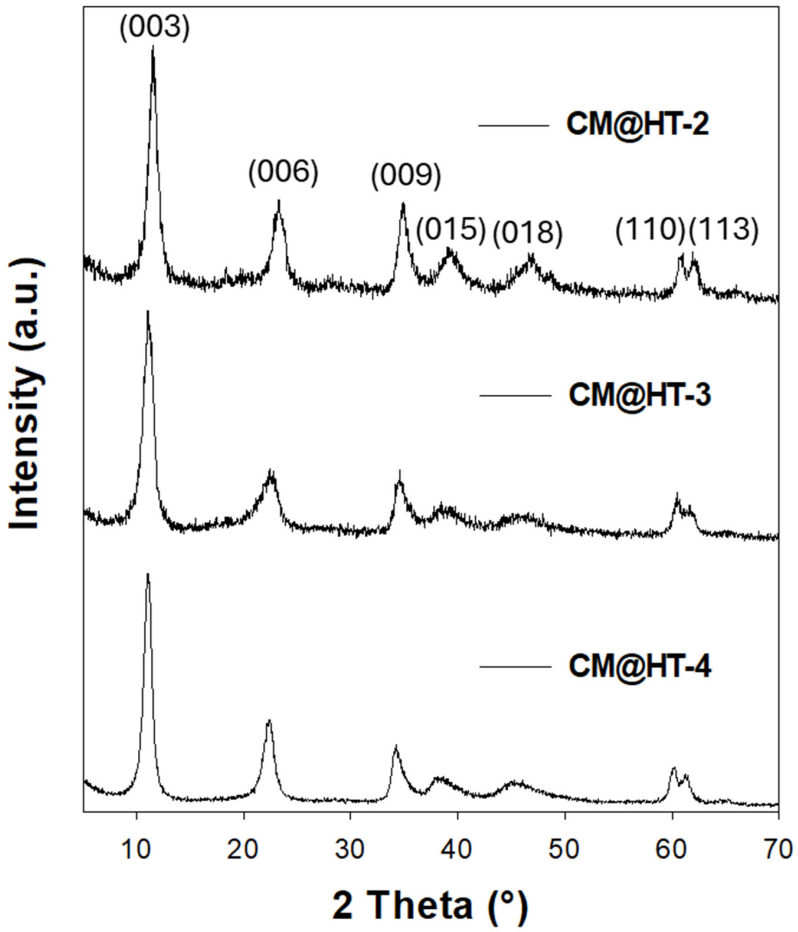

Figure 2. XRD patterns for catalysts CM@HT-X (X is the Mg/Al ratio).

Table 1 lists the parameters of the hexagonal cells c and a, calculated from the XRD patterns shown. The d_{003} values, determined using Bragg's law, range from 0.78 to 0.79 nm, with very similar values among the materials, demonstrating the presence of the same anions in the interlayer region [34,35]. This information is corroborated by the c parameter, which represents the distance between layers, where we observe similar values close to 2.3 Å. However, a slight increase in the a parameter, corresponding to the distance between cations, was observed, consistent with the increase in the Mg/Al ratio in the materials. Numerous publications have demonstrated that an increase in the concentration of divalent metal in the material leads to an increase in the distance between cations [32,36]. Finally, Table 1 shows the crystallite sizes of the different solids, calculated based on the intensity and width of the peaks. The average crystallite size for each material was determined using the Debye–Scherrer equation, considering the (003) and (006) diffraction lines [33]. As can be observed, the crystallite size was similar across the different materials, suggesting that the growth of the layers is independent of the metal ratio used in the synthesis process. In all cases, the syntheses conducted in the presence of carbon microbeads resulted in materials with lower crystallinity compared to those produced by a standard method. This has been confirmed by other studies, which use starches as structure-directing agents [37].

Figure 3 shows the IR spectra of the synthesized materials in the wavenumber range of 400−4000 cm^{-1}. As can be seen, all spectra correspond to hydrotalcite-type materials [38]. In the first region of the spectra, between 3800 and 3000 cm^{-1}, we observe typical peaks for O−H stretching vibrations associated with absorbed water and hydroxyl groups in the hydrotalcites. Additionally, a smaller peak appears around 1626 cm^{-1} in the 1200–1800 cm^{-1} region, associated with the bending mode of interlayer water. The most intense band at 1370 cm^{-1} can be assigned to carbonate anions in the intermediate layers (chelating or bridging bidentate). Finally, lower intensity bands appear between 500 and 800 cm^{-1}. The peak around 650 cm^{-1} (ν4) is attributed to in-plane bending of the carbonate ions [38]. As the Mg/Al molar ratio in the hydrotalcite increases, this peak broadens, indicating changes in the local environment of the carbonate ions, likely due to variations in the arrangement and interactions of Mg and Al ions within the hydrotalcite structure [39]. On the other hand, the band at 555 cm^{-1} is attributed to the translational modes of hydroxyl groups, influenced by Al^{3+} cations (Mg/Al−OH translation) [38].

Figure 4 illustrates SEM and TEM images confirming the deposition of layered double hydroxides onto the carbon microspheres. As previously demonstrated, the synthesis pH of nine promotes a slow, horizontal laminar growth on the carbon microspheres, resulting in their encapsulation beneath hydrotalcite layers [28]. However, the growth of hydrotalcite on the microspheres appears irregular, varying with the metal ratio. At a Mg/Al ratio of two, the microspheres exhibit sparse coating, indicative of irregular hydrotalcite growth as depicted in the SEM image. This irregular growth corroborates the presence of multiple crystalline phases in the material, as observed in the XRD study (see Figure 2). Nevertheless, evidence suggests that the layers form parallel to the carbonaceous surface of the microspheres. At a ratio of three, the microspheres are fully coated with HT layers. While a uniform coating begins throughout the material, the layers are partially separated from the material. This results in the coexistence of crystalline hydrotalcite phase adhered horizontally to the carbonaceous material and a semi-perpendicular phase, confirming that the coating is complete around the sphere, but it is not entirely uniform. Increasing the metal ratio to four results in materials that are exceptionally well-coated and compact, as shown in the TEM image in Figure 4. The carbon microspheres are entirely enveloped in HT exhibiting a compact structure, ensuring complete and thorough encapsulation of the material. This indicates a significant improvement in the coating process, with the higher metal ratio facilitating a more uniform and comprehensive coverage of the microspheres. Additionally, this improvement in the metal ratio also contributes to better crystallinity of the material, ensuring that the crystalline phases are more defined and consistent throughout the microspheres.

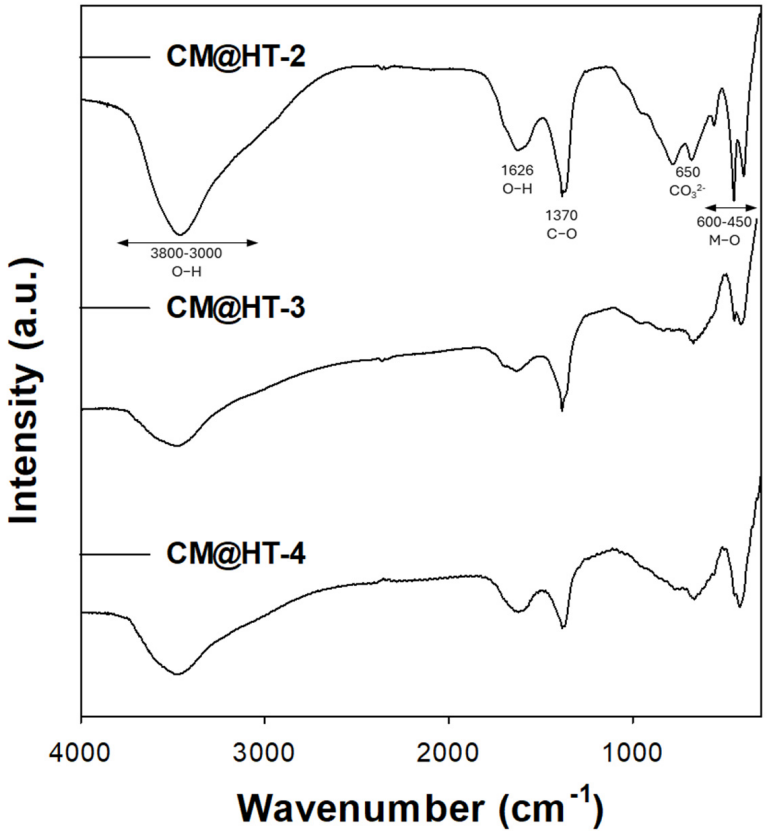

Figure 3. FTIR spectra for catalysts CM@HT-X (X is the Mg/Al ratio).

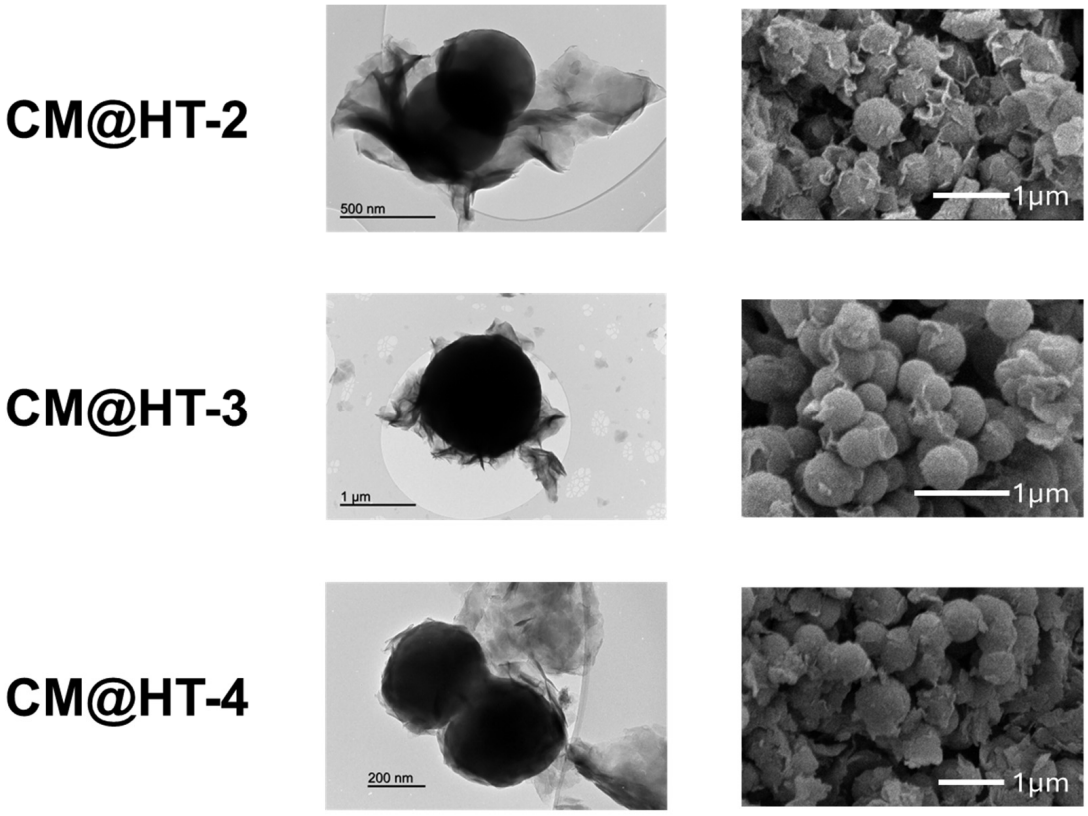

Figure 4. TEM and SEM images for catalysts CM@HT-X (X is the Mg/Al ratio).

3.2. Catalytic Evaluation

To analyze the catalytic performance in Baeyer–Villiger reactions, CM@HT samples were tested for the oxidation of cyclohexanone to ε-caprolactone using hydrogen peroxide (H_2O_2) and benzonitrile (PhCN) in aqueous solution. Under these conditions, H_2O_2 and PhCN were used in at least a 10-fold excess to ensure the reaction proceeded under pseudo-first-order kinetics for cyclohexanone, allowing the kinetic law to be simplified to:

$$v = k[\text{cyclohexanone}]$$

and making the results solely dependent on changes in cyclohexanone conversion. The presence of nitrile and hydrogen peroxide is crucial for the BV reaction to take place [15,18].

Moreover, in all reactions, a direct correlation was observed between the natural logarithm of the cyclohexanone concentration and the reaction time. Figure 5 illustrates the correlation between the natural logarithm of cyclohexanone and time for the different synthesized materials. As previously mentioned, this correlation is linear, indicating that the reaction rate follows first-order kinetics with respect to the concentration of cyclohexanone.

$$Ln\left(\frac{C_0}{C}\right) = kt$$

where C_0 and C are the cyclohexanone concentrations at times zero and t, respectively, k is the rate constant, and t is the time.

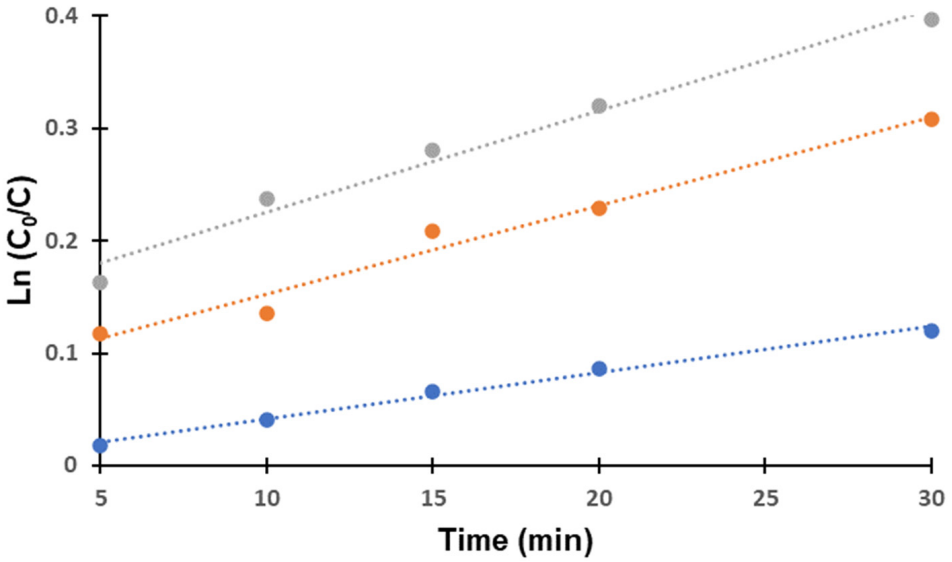

Figure 5. Correlation observed between the natural logarithm of the cyclohexanone concentration and the reaction time to short reactions times. CM@HT-2 (blue); CM@HT-3 (orange) and CM@HT-4 (gray).

Table 2 presents cyclohexanone conversion after 24 h, selectivity towards ε-caprolactone, and the rate constant for three Mg-Al hydrotalcite-coated carbon microsphere catalysts with different metal ratios. All three catalysts proved effective in the reaction. The rate constant was determined from the initial slope of ε-caprolactone formation over low conversion times, exhibiting nearly linear regression. These results indicate 100% selectivity of the catalysts towards ε-caprolactone. Minor variations in conversion among the three materials at 24 h were observed, showing an increase in ε-caprolactone conversion correlated with the metal ratio, with the highest value corresponding to CM@HT-4. This outcome was anticipated, as catalytic performance in the Baeyer–Villiger reaction with MgAl hydrotalcite-type catalysts improves with higher Mg content, as indicated by Olszówka [32].

Table 2. Conversion to ε-caprolactone in the Baeyer–Villiger oxidation of cyclohexanone.

Catalyst	Conversion (%) [a]	Selectivity [b]	Time (h)	k (10^{-3})(min^{-1}) [c]
CM@HT-2	54	100	24	1.8
CM@HT-3	57	100	24	6.7
CM@HT-4	64	100	24	7.8

[a] conversion to 6 h, [b] Selectivity to lactone, and [c] rate constant.

However, there is a noticeable increase in the rate constant of the materials when transitioning from a Mg/Al ratio of two to three, as depicted more clearly in Figure 6, which illustrates catalyst conversion at short reaction times. This improvement in the rate constant could be attributed to an enhancement in the coating of the carbon microspheres, thereby improving the catalytic process. In the case of the CM@HT-2 catalyst, as observed in Figure 4, it exhibits a heterogeneous coating, with a mixture of crystalline phases partly adhered to the carbon microspheres and others growing independently. Furthermore, the effect of ratio 2 has also been confirmed through X-ray diffraction (XRD) analysis, as shown in Figure 2. Comparing ratios 3 and 4, where the complete coating is observed in both cases, CM@HT-4 displays a more homogeneous and compact coverage. This uniform coating indicates that the HT crystals surrounding the carbon spheres align more closely and parallel to their surfaces—resulting in a material with more consistent crystallinity. While crystal size is similar across all materials, the crystalline morphology of the HTs, both in their coverage of the carbon spheres and their directional growth, significantly influences catalytic conversion rates.

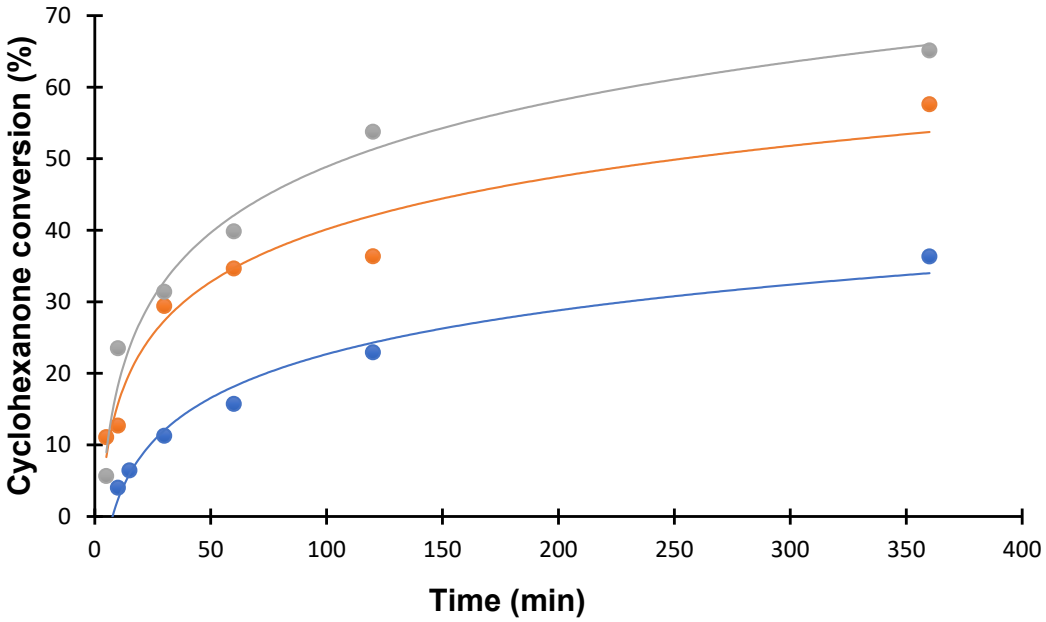

Figure 6. Cyclohexanone conversion to short reactions times. CM@HT-2 (blue); CM@HT-3 (orange) and CM@HT-4 (gray).

3.3. Reaction Mechanism

In our previous research, we developed a mechanism to explain Baeyer−Villiger oxidation reactions using hydrotalcites as catalysts [7,18]. This mechanism, outlined in Scheme 1, consists of two consecutive stages. Initially, Bronsted basic sites on the catalyst surface are attacked by hydrogen peroxide, which adsorbs onto the material to form a hydroperoxide species. This species then reacts with benzonitrile molecules, forming a peroxycarboximidic acid intermediate (the oxidant). In the subsequent stage, an electrophilic metal site within the hydrotalcite absorbs the ketone via its carbonyl group, enabling immediate

interaction with the intermediate acid to generate a Criegee-like adduct. This mechanism resembles processes observed with homogeneous catalysts. Ultimately, the Criegee-like adduct undergoes rearrangement to form the lactone. Therefore, the surface basicity of the Mg centers in the hydrotalcite layer is a key factor in the process (Scheme 1). However, as observed, hydrotalcite catalysts that have been uniformly and compactly coated onto carbon microspheres show an improvement in the catalytic process, indicating a more homogeneous crystalline structure in the materials.

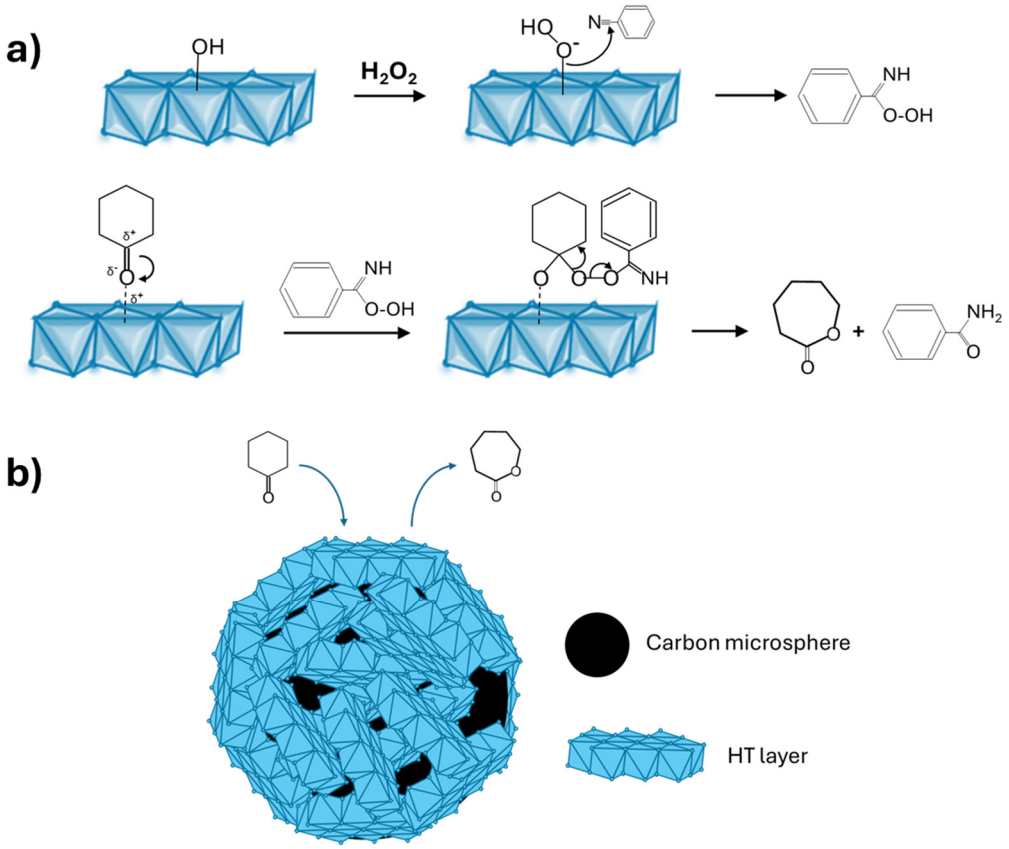

Scheme 1. (**a**) Mechanism for the Baeyer–Villiger reaction of cyclohexanone with hydrotalcites composites (CM@HT) and (**b**) the Catalyst structure.

4. Conclusions

In conclusion, this study highlights the importance of heterogeneous catalysts in advancing sustainable chemical processes. Layered materials with varying metal cation ratios and three-dimensional hierarchical structures were synthesized using carbon spheres as supports, facilitating straightforward catalyst optimization. Different characterization techniques consistently revealed a hydrotalcite-like structure in the materials. Additionally, it was observed that the synthesis process was efficient across the different metal ratios used. The degree of coating was assessed using SEM and TEM, showing that the material CM@HT-4 exhibited a more complete and homogeneous crystalline coating.

In the Baeyer–Villiger reaction under optimal conditions, the effect of crystalline growth in the coating process significantly influenced catalytic performance. Notably, the size of the crystallites had minimal impact on catalytic efficacy. However, the material CM@HT-4, which had a more homogeneous and compact coating, exhibited superior catalytic activity, highlighting the parallel growth of hydrotalcite crystals along the surface of the carbon spheres. These findings emphasize the importance of crystalline growth in the hierarchical structuring of hydrotalcite-like materials on carbon spheres and their potential use as catalysts in the Baeyer–Villiger reaction.

Supplementary Materials: The following supporting information can be downloaded at: https://www.mdpi.com/article/10.3390/cryst14100878/s1, Figure S1. XRF spectra obtained

Author Contributions: M.E.-R., D.C. and J.R.R. carried out all sampling and processing. D.C. and J.R.R. analyzed and interpreted the data. D.C., F.J.R.-S., D.E. and J.R.R. reviewed the manuscript All authors have read and agreed to the published version of the manuscript.

Funding: This research received no external funding.

Data Availability Statement: Data will be made available on request.

Acknowledgments: The authors wish to acknowledge funding by the Andalusian Regional Government (Project ProyExcel_00492), the Spanish Ministry of Science and Innovation (PID2022–142657OB-I00), and FEDER. D. C. acknowledges the FEDER funds for Programa Operativo Fondo Social Europeo (FSE) de Andalucía (PP2F_L1_07).

Conflicts of Interest: The authors declare no conflicts of interest.

References

1. Anastas, P.; Warner, J. *Green Chemistry. Theory and Practice*; Oxford university press: Oxford, UK, 1998.
2. Baeyer, A.; Villiger, V. Einwirkung Des Caro'schen Reagens Auf Ketone. *Berichte Dtsch. Chem. Ges.* **1899**, *32*, 3625–3633. [CrossRef]
3. Latos, P.; Brzęczek-Szafran, A.; Krzywiecki, M.; Pawlyta, M.; Jakóbik-Kolon, A.; Kolanowska, A.; Chrobok, A. Highly Active and Stable Catalysts for Baeyer–Villiger Oxidation—Traditional Postloading vs in Situ Synthesis of Fe/N/C Nanoparticles. *Appl. Catal. A Gen.* **2023**, *651*, 119027. [CrossRef]
4. Yan, F.; Li, C.; Liang, X.; Guo, S.; Fu, Y.; Chen, L. Baeyer-Villiger Reaction in Different Catalysis. *Recent Pat. Chem. Eng.* **2013**, *6*, 43–56. [CrossRef]
5. Ma, J.; Wu, Y.; Pan, Q.; Wang, X.; Li, X.; Li, Q.; Xu, X.; Yao, Y.; Sun, Y. The Al-Containing Silicates Modified with Organic Ligands and SnO_2 Nanoparticles for Catalytic Baeyer-Villiger Oxidation and Aerobic Carboxylation of Carbonyl Compounds. *Nanomaterials* **2023**, *13*, 433. [CrossRef] [PubMed]
6. Gorlova, O.; Paterova, I.; Karlikova, K.; Vesely, M.; Cerveny, L. Synthesis, Modification and Application of Layered Double Hydroxides as Catalysts for Baeyer-Villiger Oxidation. *Catal. Today* **2022**, *390*, 69–77. [CrossRef]
7. Karcz, R.; Olszówka, J.E.; Napruszewska, B.D.; Kryściak-Czerwenka, J.; Serwicka, E.M.; Klimek, A.; Bahranowski, K. Combined H_2O_2/Nitrile/Bicarbonate System for Catalytic Baeyer-Villiger Oxidation of Cyclohexanone to ε-Caprolactone over Mg–Al Hydrotalcite Catalysts. *Catal. Commun.* **2019**, *132*, 105821. [CrossRef]
8. Gorlova, O.; Pribylova, P.; Vyskocilova, E.; Peroutkova, K.; Kohout, J.; Paterova, I. New Sn-Mg-Al Hydrotalcite-Based Catalysts for Baeyer-Villiger Oxidation of β-Cyclocitral. *Catal. Today* **2024**, *427*, 114440. [CrossRef]
9. Korolova, V.; Dubnová, L.; Veselý, M.; Lhotka, M.; Kikhtyanin, O.; Kubička, D. On the Influence of Synthetic Parameters on the Properties and Aldol Condensation Performance of the MgAl Mixed Oxides and Rehydrated Hydrotalcites. *Appl. Clay Sci.* **2024**, *249*, 107263. [CrossRef]
10. Gorlova, O.; Pálková, S.; Kocík, J.; Tišler, Z.; Paterová, I. Baeyer-Villiger Oxidation of Myrtenal over Hydrotalcites Based Catalysts: The Role of Structure Type, Metal Content, Preparation Method and Acid-Base Properties. *Appl. Catal. A Gen.* **2024**, *671*, 119573. [CrossRef]
11. Cosano, D.; Esquivel, D.; Romero-Salguero, F.J.; Jiménez-Sanchidrián, C.; Ruiz, J.R. Use of Raman Spectroscopy to Assess Nitrate Uptake by Calcined LDH Phases. *Colloids Surf. A Physicochem. Eng. Asp.* **2020**, *602*, 125066. [CrossRef]
12. Mohapi, M.; Sefadi, J.S.; Mochane, M.J.; Magagula, S.I.; Lebelo, K. Effect of LDHs and Other Clays on Polymer Composite in Adsorptive Removal of Contaminants: A Review. *Crystals* **2020**, *10*, 957. [CrossRef]
13. Bernard, E.; Zucha, W.J.; Lothenbach, B.; Mäder, U. Stability of Hydrotalcite (Mg-Al Layered Double Hydroxide) in Presence of Different Anions. *Cem. Concr. Res.* **2022**, *152*, 106674. [CrossRef]
14. Dong, Y.; Kong, X.; Luo, X.; Wang, H. Adsorptive Removal of Heavy Metal Anions from Water by Layered Double Hydroxide: A Review. *Chemosphere* **2022**, *303*, 134685. [CrossRef]
15. Cosano, D.; Esquivel, D.; Montes, V.; Mora, M.; Romero-Salguero, F.J.; Jiménez-Sanchidrián, C.; Rafael Ruiz, J. Structural, Textural, Surface Basic and Catalytic Properties of an Aged Mg/Al Layered Double Hydroxide and Its Calcination Products. *Inorg. Chem. Commun.* **2023**, *150*, 110546. [CrossRef]
16. Kameliya, J.; Verma, A.; Dutta, P.; Arora, C.; Vyas, S.; Varma, R.S. Layered Double Hydroxide Materials: A Review on Their Preparation, Characterization, and Applications. *Inorganics* **2023**, *11*, 121. [CrossRef]
17. Jiménez-Sanchidrián, C.; Hidalgo, J.M.; Llamas, R.; Ruiz, J.R. Baeyer-Villiger Oxidation of Cyclohexanone with Hydrogen Peroxide/Benzonitrile over Hydrotalcites as Catalysts. *Appl. Catal. A Gen.* **2006**, *312*, 86–94. [CrossRef]
18. Ruiz, J.R.; Jiménez-Sanchidrián, C.; Llamas, R. Hydrotalcites as Catalysts for the Baeyer-Villiger Oxidation of Cyclic Ketones with Hydrogen Peroxide/Benzonitrile. *Tetrahedron* **2006**, *62*, 11697–11703. [CrossRef]
19. Tichit, D.; Layrac, G.; Alvarez, M.G.; Marcu, I.C. Formation Pathways of MII/MIII Layered Double Hydroxides: A Review. *Appl. Clay Sci.* **2024**, *248*, 107234. [CrossRef]

20. Tu, Q.; Zhang, Q.; Sun, X.; Wang, J.; Lin, B.; Chen, L.; Liu, J.; Deng, Z. Construction of Three-Dimensional Nickel-Vanadium Hydrotalcite with Ball-Flower Architecture for Screen-Printed Asymmetric Supercapacitor. *Appl. Surf. Sci.* **2023**, *615*, 156347. [CrossRef]
21. Jia, Z.; Ji, N.; Diao, X.; Li, X.; Zhao, Y.; Lu, X.; Liu, Q.; Liu, C.; Chen, G.; Ma, L.; et al. Highly Selective Hydrodeoxygenation of Lignin to Naphthenes over Three-Dimensional Flower-like Ni2P Derived from Hydrotalcite. *ACS Catal.* **2022**, *12*, 1338–1356. [CrossRef]
22. Wang, G.; Huang, D.; Cheng, M.; Chen, S.; Zhang, G.; Lei, L.; Chen, Y.; Du, L.; Li, R.; Liu, Y. Metal-Organic Frameworks Template-Directed Growth of Layered Double Hydroxides: A Fantastic Conversion of Functional Materials. *Coord. Chem. Rev.* **2022**, *460*, 214467. [CrossRef]
23. Khorshidi, M.; Asadpour, S.; Sarmast, N.; Dinari, M. A Review of the Synthesis Methods, Properties, and Applications of Layered Double Hydroxides/Carbon Nanocomposites. *J. Mol. Liq.* **2022**, *348*, 118399. [CrossRef]
24. Peng, J.; Qu, H.; Si, J.; Li, S.; Zhao, L.; Wang, Y.; Liang, Q.; Zhang, W.; Wei, C.; Li, W.; et al. Protecting Mg-Sites from Hydration by Embedding Magnesium-Aluminium Layered Double Hydroxide in Halloysite and Using as Pickering Catalysts in Baeyer-Villiger Oxidation. *Appl. Clay Sci.* **2024**, *251*, 107328. [CrossRef]
25. Ye, X.; Shi, X.; Li, J.; Jin, B.; Cheng, J.; Ren, Z.; Zhong, H.; Chen, L.; Liu, X.; Jin, F.; et al. Fabrication of Mg-Al Hydrotalcite/Carbon Nanotubes Hybrid Base Catalysts for Efficient Production of Fructose from Glucose. *Chem. Eng. J.* **2022**, *440*, 135844. [CrossRef]
26. Bai, Z.; Rong, D.; Li, M.; Xu, G.; Liu, S.; Zeng, J.; Lv, Y.; Tang, Y.; Wen, X. Hierarchical Mg/Al Hydrotalcite Oxide Hollow Microspheres with Excellent Adsorption Capability towards Congo Red. *Dalton Trans.* **2024**, *53*, 3744–3755. [CrossRef]
27. Li, M.; Li, W.; Liu, S. Hydrothermal Synthesis, Characterization, and KOH Activation of Carbon Spheres from Glucose. *Carbohydr. Res.* **2011**, *346*, 999–1004. [CrossRef]
28. Cosano, D.; Esquivel, D.; Puertas, A.J.; Romero-Salguero, F.J.; Jiménez-Sanchidrián, C.; Ruiz, J.R. Microstructural Analysis of 3D Hierarchical Composites of Hydrotalcite-Coated Silica Microspheres. *Microporous Mesoporous Mater.* **2021**, *323*, 111247. [CrossRef]
29. Cosano, D.; Esquivel, D.; Romero-Salguero, F.J.; Jiménez-Sanchidrián, C.; Ruiz, J.R. Three-Dimensional Hierarchical Hydrotalcite–Silica Sphere Composites as Catalysts for Baeyer–Villiger Oxidation Reactions Using Hydrogen Peroxide. *Catalysts* **2022**, *12*, 629. [CrossRef]
30. Gil-Gavilán, D.G.; Cosano, D.; Castillo-Rodríguez, M.; de Miguel, G.; Esquivel, D.; Jiménez-Sanchidrián, C.; Ruiz, J.R.; Romero-Salguero, F.J. Composites of Co-Al Hydrotalcites and Carbon Nanomaterials for Photocatalytic H_2 Production. *Appl. Clay Sci.* **2023**, *238*, 106924. [CrossRef]
31. Kızılduman, B.K.; Turhan, Y.; Doğan, M. Mesoporous Carbon Spheres Produced by Hydrothermal Carbonization from Rice Husk: Optimization, Characterization and Hydrogen Storage. *Adv. Powder Technol.* **2021**, *32*, 4222–4234. [CrossRef]
32. Olszówka, J.; Karcz, R.; Napruszewska, B.D.; Duraczyńska, D.; Gaweł, A.; Bahranowski, K.; Serwicka, E.M. Baeyer-Villiger Oxidation of Cyclohexanone with H_2O_2/Acetonitrile over Hydrotalcite-like Catalysts: Effect of Mg/Al Ratio on the ε-Caprolactone Yield. *Catal. Commun.* **2017**, *100*, 196–201. [CrossRef]
33. Cavani, F.; Trifiro, F.; Vaccari, A. Hydrotalcite-Type Anionic Clays: Preparation, Properties and Applications. *Catal. Today* **1991**, *11*, 173–301. [CrossRef]
34. Zhou, H.; Jiang, Z.; Wei, S. A New Hydrotalcite-like Absorbent FeMnMg-LDH and Its Adsorption Capacity for Pb^{2+} Ions in Water. *Appl. Clay Sci.* **2018**, *153*, 29–37. [CrossRef]
35. Lin, J.; Zhang, Y.; Zhang, Q.; Shang, J.; Deng, F. Enhanced Adsorption Properties of Organic ZnCr-LDH Synthesized by Soft Template Method for Anionic Dyes. *Environ. Sci. Pollut. Res.* **2021**, *28*, 48236–48252. [CrossRef] [PubMed]
36. Olszówka, J.E.; Karcz, R.; Bielańska, E.; Kryściak-Czerwenka, J.; Napruszewska, B.D.; Sulikowski, B.; Socha, R.P.; Gaweł, A.; Bahranowski, K.; Olejniczak, Z.; et al. New Insight into the Preferred Valency of Interlayer Anions in Hydrotalcite-like Compounds: The Effect of Mg/Al Ratio. *Appl. Clay Sci.* **2018**, *155*, 84–94. [CrossRef]
37. Michalik, A.; Napruszewska, B.D.; Walczyk, A.; Krysciak-Czerwenka, J.; Duraczynska, D.; Serwicka, E.M. Synthesis of Nanocrystalline Mg-Al Hydrotalcites in the Presence of Starch-the Effect on Structure and Composition. *Materials* **2020**, *13*, 602. [CrossRef]
38. Karcz, R.; Napruszewska, B.D.; Walczyk, A.; Kryściak-Czerwenka, J.; Duraczyńska, D.; Płaziński, W.; Serwicka, E.M. Comparative Physicochemical and Catalytic Study of Nanocrystalline Mg-Al Hydrotalcites Precipitated with Inorganic and Organic Bases. *Nanomaterials* **2022**, *12*, 2775. [CrossRef]
39. Sharma, S.K.; Kushwaha, P.K.; Srivastava, V.K.; Bhatt, S.D.; Jasra, R.V. Effect of Hydrothermal Conditions on Structural and Textural Properties of Synthetic Hydrotalcites of Varying Mg/Al Ratio. *Ind. Eng. Chem. Res.* **2007**, *46*, 4856–4865. [CrossRef]

Disclaimer/Publisher's Note: The statements, opinions and data contained in all publications are solely those of the individual author(s) and contributor(s) and not of MDPI and/or the editor(s). MDPI and/or the editor(s) disclaim responsibility for any injury to people or property resulting from any ideas, methods, instructions or products referred to in the content.